American Mineralogist, Volume 97, pages 164–175, 2012

Oxide melt solution calorimetry of Fe^{2+}-bearing oxides and application to the magnetite–maghemite (Fe_3O_4–$Fe_{8/3}O_4$) system

Kristina I. Lilova,[1] Fen Xu,[1] Kevin M. Rosso,[2] Carolyn I. Pearce,[2] Saeed Kamali,[3] and Alexandra Navrotsky[1,*]

[1]Peter A. Rock Thermochemistry Laboratory and NEAT ORU, University of California at Davis, Davis, California 95616, U.S.A.
[2]Pacific Northwest National Laboratory, Richland, Washington 99352, U.S.A.
[3]Department of Applied Science, University of California at Davis, Davis, California 95616, U.S.A.

Abstract

A consistent methodology for obtaining the enthalpy of formation of Fe^{2+}-containing binary and multicomponent oxides using high-temperature oxide melt solution calorimetry has been developed. The enthalpies of wüstite (FeO) and magnetite (Fe_3O_4) oxidation to hematite (Fe_2O_3) were measured using oxidative drop solution calorimetry in which the final product is dissolved ferric oxide. Two methods were applied: drop solution calorimetry at 1073 K in lead borate solvent and at 973 K in sodium molybdate, each under both oxygen flowing over and bubbling through the solvent, giving consistent results in agreement with literature values. The enthalpies of formation of all three iron oxides from the elements were obtained using a thermodynamic cycle involving the directly measured oxidative dissolution enthalpy of iron metal in sodium molybdate at 973 K and gave excellent consistency with literature data.

The methodology was then applied to the magnetite–maghemite system. The enthalpy of mixing of the Fe_3O_4–$Fe_{8/3}O_4$ spinel solid solution is exothermic and, represented by a subregular (Margules) formalism, $\Delta H_{mix} = x(1-x)[-63.36 \pm 8.60(1-x) + 17.65 \pm 6.40x]$ kJ/mol, where x is the mole fraction of magnetite. The entropies of mixing of the solid solution were calculated for different assumptions about the distribution of cations, charges, and vacancies in these defect spinels. The different models lead to only small differences in the entropy of mixing. Calculated free energies of mixing show no evidence for a solvus in the magnetite–maghemite system.

Keywords: Iron-bearing oxides, magnetite-maghemite spinel solid solution, enthalpies of mixing, vacancy distribution, high-temperature oxide melt solution calorimetry

Introduction

Iron oxides are widespread in all parts of the global system as minerals in soils, sediments, and rocks in the lithosphere, as particles in the atmosphere and hydrosphere, and in organisms ranging from bacteria to pigeons in the biosphere (Cornell and Schwertmann 2003). Iron oxides are found on the surface of Mars (Morris et al. 2000). They are often products of corrosion of steel or traces of iron meteorites (Cook et al. 1999; Dunn et al. 2000; Noguchi and Nakamura 2000). Wüstite ($Fe_{1-x}O$) is an end-member of the magnesiowüstite solid solution phase in the Earth's lower mantle (Lindsley 1991). Ringwood (1977) proposed a model for the Earth's core with FeO as the major light component. These widespread applications lend great importance to fundamental thermodynamic studies of the Fe-O system to understand core formation and core-mantle interactions. The variation of the properties in magnetic minerals provides one of the most complete records of geological and geomagnetic field history as well as information about palaeoclimate (Van Oorschot and Dekkers 1999). Magnetite (Fe_3O_4) and maghemite (γ-Fe_2O_3 or $Fe_{8/3}O_4$), the reduced and oxidized end-members of a spinel solid solution, are widely used in ceramic processing, magnetic data storage, catalysis, and microwave radiation shielding (Cornell and Schwertmann 2003). Additionally, magnetite is a corrosion product in the steel containers used for the long-term storage of nuclear waste (Neff et al. 2004). The Fe^{2+} ions in the structure make magnetite a useful reductant for heavy metals, radionuclides, and other toxic compounds (Peterson et al. 1997; White and Peterson 1996; Scott et al. 2005). Maghemite is often an intermediate phase in the oxidation of magnetite to hematite (Gallagher et al. 1968, 1970; Shebanova and Lazor 2003; Gillot et al. 1978; Goss 1988).

Stoichiometric magnetite Fe_3O_4 has an inverse spinel structure with one Fe^{3+} per formula unit on tetrahedral sites and Fe^{2+} and the remaining Fe^{3+} randomly distributed on the octahedral sites: $Fe^{3+}[Fe^{2+}Fe^{3+}]O_4$. The structure was originally suggested by Verwey and de Boer (1936) to account for its anomalously high room-temperature electrical conductivity through continuous exchange of electrons between Fe^{2+} and Fe^{3+} on the octahedral sites. Later, the fast electron hopping hypothesis was supported by Mössbauer studies (Bauminger et al. 1961). The nature of this exchange process has been interpreted either as a thermally activated hopping process or as a global delocalization of the sixth 3d electron of the Fe^{2+} ions into a conduction band involving the entire octahedral sublattice (Vandenberghe and De Grave 1989). Non-stoichiometric magnetite can be represented as $Fe_{3-y}O_4$

* E-mail: anavrotsky@ucdavis.edu

0003-004X/12/0001–164$05.00/DOI: http://dx.doi.org/10.2138/am.2012.3883

where y ranges between zero (magnetite) and 0.333 (maghemite).

Maghemite (magnetite–hematite) γ-Fe_2O_3 or $Fe_{8/3}O_4$ has a defect spinel structure with one third mole of cation vacancies per four moles of oxygen, compensating for the oxidation of Fe^{2+} (Cornell and Schwertmann 2003). Variations in the maghemite structure and the distribution of vacancies depend mainly on the method of preparation. It has been suggested that the vacancies can be distributed at random (cubic space group), ordered as the lithium cations in $LiFe_5O_8$ (space group $P4_132$), or with an ordered distribution with tetragonal symmetry (space group $P4_32_12$) (Hägg 1935; Verwey 1939; Haul and Schoon 1939; Néel 1948; Braun 1952; Sinha and Sinha 1957; Ferguson and Hass 1958; Oosterhout and Rooijmans 1958; Ueda and Hasegawa 1962; Armstrong et al. 1966; Takei and Chiba 1966; Kullerud et al. 1969; Coey and Morrish 1971; Weber and Hafner 1971; Annersten and Hafner 1973; Greaves 1983; Cormack 1983; Boudeulle et al. 1983; Kryukova et al. 1990; Da Costa et al. 1994, 1998; Morales et al. 1994; Shmakov et al. 1995; Belin et al. 2002).

The thermodynamic properties of bulk wüstite, magnetite, and hematite are well established (Darken and Gurry 1946; Raccah and Vallet 1962; Vallet et al. 1963; Komarov et al. 1967; Rizzo et al. 1968, 1969; Westrum and Groenvold 1969; Marucco et al. 1970; Janowski et al. 1970a, 1970b; Asao et al. 1970; Goursat and Smeltzer 1973; Groenvold and Sveen 1974; Vallet 1975a, 1975b; Kurepin 1975; Spencer et al. 1978; Carel and Vallet 1981; Esdaile 1983; Vallet and Carel 1986; Holland and Powell 1998; Berman 1988; Hemingway 1990; Lindsley 1991; Sundman 1991; Takai et al. 1994; Stolen et al. 1996; Fabrichnaya and Sundman 1997; Haavik et al. 2000; Leonovich et al. 2001; Cornell and Schwertmann 2003; Snow et al. 2010). Previous solution calorimetric studies on maghemite of different particle size have been performed by high-temperature oxide melt calorimetry at 973 K using sodium molybdate as solvent (Laberty and Navrotsky 1998; Bomati-Miguel et al. 2008) and acid solution calorimetry (Majzlan et al. 2003). However, oxide melt solution calorimetry of materials containing ferrous iron or a mixture of ferrous and ferric iron has not been straightforward. There are no thermochemical measurements on the magnetite–maghemite solid solution and, indeed, thermochemical data for spinel solid solutions, in which magnetite is a component, are far more sparse and less certain than those for other spinel systems. The purpose of the present study is twofold. First, we develop an oxide melt solution calorimetric protocol for mixed Fe^{2+}, Fe^{3+} phases and validate it by a calorimetric study of wüstite, magnetite, and hematite. Second, we apply the methodology to the magnetite–maghemite solid solution. This methodology will make possible the study of enthalpies of formation of many other mixed valence iron systems at both bulk and nanoscales.

Oxide-melt solution calorimetry of iron-bearing phases

Because many iron-bearing phases (aluminates, silicates, titanates) do not dissolve readily in aqueous solvents, high-temperature oxide melt solution calorimetry is the method of choice. In this method, small samples of solid are dissolved in a large volume of molten solvent, and the difference in the enthalpy of solution of the reactants and products gives the enthalpy of reaction, e.g., formation of a ternary compound or solid solution from binary oxide end-members. For such a calculation to be valid, one must be certain the initial state of the oxides immediately prior to dissolution is known and the final state of the oxides in the melt is well defined and reproducible. Prior to the mid 1990s, most oxide melt solution calorimetry was done by the "solution" method in which a powdered sample was suspended in a small platinum cup above the solvent in the calorimeter, equilibrated for several hours, and then dissolved by stirring the cup in the melt (Navrotsky 1977). To maintain ferrous iron in the solids at high temperature, a non-oxidizing atmosphere was required and argon gas was flushed through the calorimeter. It was hoped, but by no means proven, that oxidation of ferrous to ferric iron did not occur either prior to or during dissolution. The actual oxygen fugacity in the system was not measured and was probably controlled by the purity of the argon gas and/or small leaks in the system. Thierry et al. (1981) used such a solution method with sodium and lithium metaborate eutectic ($NaBO_2$ + $LiBO_2$) molten solvent at 1180 K under an argon atmosphere to measure the enthalpy of formation of the forsterite–fayalite (Mg_2SiO_4–Fe_2SiO_4) system. Chatillon-Colinet et al. (1983) used the same solvent and argon atmosphere to measure the enthalpy of formation of $Fe_3Al_2Si_3O_{12}$ (almandine) and five synthetic orthopyroxenes on the join $MgSiO_3$–$FeSiO_3$·PbO·B_2O_3 as a solvent and argon atmosphere was preferred by Wood and Kleppa (1981) and by Akaogi et al. (1989) for Mg_2SiO_4–Fe_2SiO_4 olivine solid solutions. The solvent was allowed to equilibrate with the argon, first outside the calorimeter and then inside to minimize the effect of any dissolved oxygen. Enthalpies of hematite–ilmenite (Fe_2O_3–$FeTiO_3$) solid solutions (Brown and Navrotsky 1994), olivine solid solution Mg_2SiO_4–Fe_2SiO_4 (Kojitani and Akaogi 1994) and $CaTiO_3$–$FeTiO_3$ (Linton et al. 1998) were measured in the same way. Solution calorimetry in PbO·B_2O_3 under argon was used to measure the enthalpies of the olivine–spinel transition in Fe_2SiO_4 (Navrotsky et al. 1979) and the enthalpies of mixing in Fe_2SiO_4–Mg_2SiO_4 spinel solid solutions (Kojitani and Akaogi 1994). However, because molten lead borate is readily reduced, there were possible parasitic side reactions, involving the formation of lead at the surface of the platinum crucibles, as well as possible small amounts of oxidation of ferrous to ferric iron; thus the actual enthalpies of solution measured in different laboratories were different. Wüstite could not be used as a solute and reference material and, though enthalpies of phase transition and mixing could be measured, enthalpies of formation were difficult to obtain.

A multistep process involving oxidation of the solid to the ferric state followed by dissolution of the oxidized product in a molten oxide solvent in an oxidizing atmosphere has been another strategy. Such measurements were performed to obtain the enthalpy of formation of $FeCO_3$ (Chai and Navrotsky 1994), in $Ca(Fe_xMg_{1-x})(CO_3)_2$ solid solution (Chai and Navrotsky 1996a) and (Fe,Mg)CO_3 solid solution (Chai and Navrotsky 1996b). Transposed-temperature drop calorimetric measurements in an argon atmosphere (no solvent present) were also performed to obtain the enthalpy of $FeTiO_3$ (Mehta et al. 1994). A calorimetric study of maghemite and goethite with different specific surface area and water content and stoichiometric magnetite has been performed by Laberty and Navrotsky (1998) using a combination of transposed temperature drop calorimetry followed drop solution calorimetry in sodium

molybdate solvent under high flow of oxygen

More recently, "drop solution calorimetry," in which a 5–10 mg pellet is dropped from room temperature into the solvent in the calorimeter, has become the preferred technique (Navrotsky 1997). It has several advantages over the older "solution calorimetry:" the structural, oxidation, and hydration states of the sample are those characterized at room temperature, several samples can be dropped without changing the sample assembly, thus leading to greater productivity, and the irreproducible effects of mechanical stirring are eliminated. Two advances have made drop solution calorimetry practical. The first is improvement in calorimeter operation leading to more stable baseline signals and reduction in uncertainties of measurements so that the larger heat effects in drop solution calorimetry compared to solution calorimetry do not compromise the accuracy of the results. The second is the introduction of stirring by bubbling gas directly through the solvent. The multistep oxidation-dissolution procedure above can be simplified to a single direct drop solution measurement with flushing and bubbling O_2 through the solvent. The bubbling gas brings the Fe^{2+}-bearing phases into much more direct contact with an oxidizing environment, speeds oxidation and stirs the solvent. These techniques were applied to $Mg_{1-x}Fe_xCa(CO_3)_2$ solid solutions (Navrotsky et al. 1999), manganese iron oxide spinels

$(Mn_xFe_{1-x})_3O_4$ (Guillemet-Fritsch et al. 2005) and binary iron nitrides (Tessier et al. 2000). This method of "oxidative drop solution calorimetry" forms the basis of the present study.

Experimental methods

Sample preparation

Dense pieces of iron metal, wüstite Fe_xO, two different samples of magnetite $Fe_{3-y}O_4$ (referred below as MM70 and MM90) and hematite Fe_2O_3 (commercial materials from Alfa Aesar and Aldrich) with purity of 99.98+%, 99.5%, 98%, 99.998%, 99.999% (metals basis), respectively, were used. Iron lumps were kept in a glovebox filled with argon. The stoichiometric magnetite was the same material prepared and described by Pearce et al. (2010).

The magnetite–maghemite solid solutions were prepared by controlled oxidation of magnetite. In general, oxidation products resulting from thermal treatment of magnetite are strongly dependent on the conditions used to perform the transformation: temperature, oxygen pressure, heating time, and particle size. Heating small particles of magnetite in air or oxygen should produce magnetite–maghemite single phase solid solutions (Gallagher et al. 1968, 1970; Shebanova and Lazor 2003; Gillot et al. 1978; Goss 1988). Because the time of reaction is relatively short, it is difficult to stop oxidation at a specific composition, especially in the magnetite-rich region. The small differences in the uniformity of the sample and the heating conditions could cause the start of transformation to hematite. Additionally, since the first stage of reaction, oxidation to maghemite, is exothermic, the emitted heat could increase the sample temperature and trigger the second stage, transformation to hematite.

To limit the reaction to spinel solid solution formation only, the synthesis of all $Fe_{3-y}O_4$ samples was performed in a vacuum furnace at a low-oxygen pressure of around 10 Pa. The temperature interval and time length were varied between 373 and 443 K and 1 to 21 days, depending on the desired composition. Even with increasing time beyond 21 days and at the highest temperature possible (limited by transformation to hematite), the most oxidized composition obtained was 82 mol% $Fe_{8/3}O_4$. Switching to higher vacuum (0.5–2 Pa) resulted in a mixture of hematite and nearly stoichiometric magnetite. Increasing the temperature between 443 and 463 K led to no change in the solid solution composition, but to an increase of the hematite content. Increasing the temperature above 463 K produced less oxidized, non-stoichiometric magnetite and noticeably larger amount of hematite.

Two commercial samples of magnetite with approximately 70.0 mol% (MM70) and 90 mol% (MM90) Fe_3O_4 were used as starting materials. The particle size was between 100 and 300 nm; water content was 0.01 and 0.1 mole, respectively. Sample MM74 was prepared from MM90, and all other solid solution samples were obtained from MM70.

Characterization

Powder X-ray diffraction. The phase purity of all samples and the lattice parameters of the solid solutions were checked by X-ray powder diffraction (XRD) using a Bruker D8 Advance diffractometer at the Peter A. Rock Thermochemistry Laboratory and NEAT ORU, University of California, Davis. The wüstite samples contained around 1.3 mol% Fe_3O_4. The magnetite–maghemite samples MM90 and MM74 contained less than 1 mol% α-Fe_2O_3.

Differential scanning calorimetry. To measure the actual stoichiometry of the iron compounds, thermogravimetric and differential thermal analysis (TG/DSC) were conducted using a Netzsch Simultaneous Thermal Analyzer (STA 449) and a Setaram Labsys Evo at the Peter A. Rock Thermochemistry Laboratory and NEAT ORU, University of California, Davis. A pellet between 30 and 40 mg was packed in a standard platinum crucible with a lid. During the first run, the loaded crucible was placed in the DSC and heated from room temperature to 973 K at 10 K/min under argon flow to get the weight change, associated with water loss. The second run was performed to 1173 K in oxygen and the weight gain of the sample was registered. The final product of oxidation, hematite, was verified using XRD.

Mössbauer spectroscopy. ^{57}Fe Mössbauer spectroscopy was performed on a SEE Co. MS4 Mössbauer spectrometer at the Department of Applied Science, University of California, Davis. The radioactive source was ^{57}Co in an Rh matrix at room temperature. The spectra were least squares fitted using Recoil software. All centroid shifts, δ, are given with respect to metallic α-iron at 298 K.

Synchrotron-based X-ray absorption and X-ray magnetic circular dichroism. The composition of three solid-solution samples was also characterized using X-ray absorption (XA) spectroscopy and X-ray magnetic circular dichroism (XMCD), an XA difference spectrum technique based on circularly polarized light absorption in alternating opposing static applied magnetic fields that is sensitive to the oxidation state and local structure of magnetically ordered iron cations at solid surfaces (Chen et al. 1995; Stohr 1995; Van der Laan et al. 1986; Van der Laan and Thole 1991). XA spectra at the Fe $L_{2,3}$ edges were obtained on beamline 4.0.2 at the Advanced Light Source (ALS), Berkeley, CA, using the eight–pole resistive magnet endstation (Arenholz and Prestemon 2005). Powder samples were loaded onto carbon tape attached to the sample manipulator. XA was monitored in total-electron yield (TEY) mode, which has an effective probing depth of 50 Å (Gota et al. 2000). Hence, in contrast to Mössbauer, these measurements emphasize the composition at or near the surface of the samples. At each energy point, XA spectra were measured for two opposite magnetization directions by reversing the applied field of 0.6 T. After normalization to the incident beam intensity, the XMCD spectrum is obtained as the difference between the two XA spectra (Pattrick et al. 2002). To obtain the cation distribution over the two structural Fe site types, the experimental XMCD was fit by means of a nonlinear least-squares analysis, using the calculated spectra for each site. In these calculations, described in Van der Laan and Kirkman (1992) and Van der Laan and Thole (1991), the 10Dq crystal field parameters were taken as 1.2 and 0.6 eV for Fe *Oh* and *Td* sites. The results were convoluted by a Lorentzian of $\Gamma = 0.3$ (0.5) eV for the L_3 (L_2) edge to account for intrinsic core-hole lifetime broadening and by a Gaussian of $\sigma = 0.2$ eV to account for instrumental broadening.

High-temperature calorimetry. High-temperature oxide melt solution calorimetry was performed using a Tian Calvet twin calorimeter described in detail by Navrotsky (1977, 1997). In the drop solution calorimetry experiment, samples in the form of pellets (around 5 mg) were dropped from room temperature (298 K) into the molten solvent at the calorimeter temperature in a platinum crucible. Oxygen gas was flushed over the solvent at 90 mL/min and bubbled through it at 5 mL/min. Two different solvents were used—sodium molybdate ($3Na_2O{\cdot}4MoO_3$) at 973 K and lead borate ($2PbO{\cdot}B_2O_3$) at 1073 K. The calorimeters were calibrated using the heat content of 5 mg α-Al_2O_3 pellets.

When attempting drop solution calorimetry under flowing and bubbling oxygen in lead borate solvent, we saw traces of a blackish discoloration on platinum crucibles at the experiments at 973 K. Although iron-bearing samples dissolved well, the data showed some scatter and we were concerned that a parasitic side reaction was occurring. We scraped off some of the black material and identified it by X-ray diffraction and microprobe analysis to be a platinum lead oxide Pb_2PtO_4. This material did not form during calorimetry under flowing and bubbling air at 973 K, and it did not form under oxygen at 1073 K. These observations are generally consistent with prior work on the stability of this compound (Bettahar et al. 1987; Jacob et al. 2009). We therefore do not recommend calorimetry at 973 K in lead borate under an oxygen atmosphere.

RESULTS AND DISCUSSION

Characterization

Powder XRD cannot be used alone for characterizing the Fe_3O_4–$Fe_{8/3}O_4$ spinels. Although the structures of magnetite and maghemite are distinct, their X-ray diffraction patterns are similar; determining the exact stoichiometry is made more difficult by peak shifting and broadening associated with solid solution and small particle-size effects. Bulk magnetic measurements alone cannot characterize partially oxidized materials, especially when both spinel and hematite are present because of the various mixtures possible between three constituents (magnetite, maghemite, and hematite).

The sensitivity of thermogravimetric analysis decreases with decreasing weight gain, resulting from the oxidation of the decreasing amount of Fe^{2+} to Fe^{3+} in maghemite-rich samples. This limitation could be partially overcome by using bigger samples and multiple runs. Adsorbed water tends to mask mass changes in thermogravimetric analysis of small particle specimens. This problem can be avoided by an initial heating in inert atmosphere, which leads to determining the amount of adsorbed water and its removal, followed by heating in oxygen, which gives the actual stoichiometry.

We therefore used a combination of techniques to obtain the phase purity, oxidation state, and water content of our samples. We were also concerned about sample homogeneity, especially for the partially oxidized magnetite, since TG/DSC and Mössbauer spectroscopy provide only the total Fe^{2+} content in the sample, which could be a zoned or even mechanical mixture of two solid solutions. Synthesis methods, using controlled oxidation of magnetite and magnetite-rich solid solutions as well as controlled reduction of maghemite to $Fe_{3-y}O_4$ solid solutions and characterization of the final products are often described in the literature without providing evidence about the homogeneity of the sample. For example, Schmidbauer and Keller (2006) assumed that long reaction times, a thin layer of sample and small (less than 300 nm) magnetite particles can assure the formation of homogeneous magnetite–maghemite solid solution.

In this work, all $Fe_{3-y}O_4$ samples were first characterized by XRD and TG/DSC. In addition, selected sample (see Table 1) were studied by Mössbauer spectroscopy and XMCD. The XMCD might detect any differences between surface and bulk composition and was used to verify the homogeneity by measuring different spots on the selected sample (100×100 μm). Overall agreement among these methods is satisfying and suggests no major heterogeneity. The compositions obtained by each method, and the best estimate of the composition, taken as an average of these values, are shown in Table 1.

The lattice parameters of the solid solutions and magnetite end-member were determined by Rietveld refinement (ICDD PDF Card No. 19-0629). The pure maghemite lattice parameter is taken from ICDD PDF Card No. 39-1346. The variation of lattice parameters with the Fe^{2+} content in the solid-solution series is shown in Figure 1 and compared with experimental results by Schmidbauer and Keller (2006) and Fukasawa et al. (1993). Good agreement is observed between 40 and 100 mol% of magnetite; there are no compositions between 18 and 40 mol% except one value below 10 mol%, which is slightly higher. Although there may be a small positive deviation from linearity in lattice parameters, Vegard's law is a good approximation when experimental errors are considered.

MM48, MM70, and MM90 samples were characterized by Mössbauer spectroscopy (Fig. 2) and compared with stoichiometric magnetite (Kündig and Hargrove 1969). Due to overlap of the signal from maghemite and the signal from the tetrahedral site (Td) in magnetite, the spectrum from MM48 was fitted with four sextets by locking the hyperfine parameters for the latter. The first sextet with B_{hf1} of 50 T is from maghemite with an intensity of 42%. The second sextet with B_{hf2} of 48.9 T and an intensity of 16% is from the tetrahedral site of magnetite. The third sextet with B_{hf3} of 45.8 T and δ of 0.64 mm/s is typical for Fe in the octahedral site (Oh) of magnetite. The intensity of the octahedral sextet is just 17%, whereas it should be approximately double the intensity of the tetrahedral site, i.e., 32%. To account for this discrepancy, the fourth sextet, with reduced B_{hf4}, 40.3 T, and very broad distribution σ_4 (11.1 T), should mostly consist of the Fe signal from octahedral sites and partially from maghemite. A δ value of 0.58 mm/s supports this conclusion. Due to this broad sextet, the uncertainty in intensities is high, but with this description, the sample should consist of around 48% magnetite and 52% of maghemite.

The MM70 sample also consists of four sextets with almost the same hyperfine parameters but different intensities (Fig. 2). With the same argument, the sample should consist of 72% magnetite and 28% maghemite.

The MM90 sample spectrum is much "cleaner" and can be

TABLE 1. Average stoichiometry and mole fraction Fe_3O_4 of Fe_3O_4–$Fe_{8/3}O_4$ solid solutions and techniques used for characterization of each sample

Sample	Average $Fe_{3-y}O_4$ composition	Average mole fraction $Fe_3O_4 \pm 0.03$*	Techniques			
			Labsys Evo (TGA)	Netzsch STA 449 (TGA)	XMCD	Mössbauer spectroscopy
MM18	$Fe_{2.727\pm0.003}O_4$	0.180	0.180 ± 0.010†			
MM24	$Fe_{2.743\pm0.013}O_4$	0.227	0.251 ± 0.017†		0.204 ± 0.015†	
MM33	$Fe_{2.777\pm0.004}O_4$	0.330	0.330 ± 0.012†			
MM40	$Fe_{2.803\pm0.010}O_4$	0.408	0.423 ± 0.003†	0.380		
MM48	$Fe_{2.826\pm0.003}O_4$	0.478	0.477 ± 0.009†			0.480
MM54	$Fe_{2.846\pm0.005}O_4$	0.540	0.550		0.530 ± 0.001†	
MM59	$Fe_{2.863\pm0.006}O_4$	0.589	0.590 ± 0.017†	0.586		
MM70	$Fe_{2.900\pm0.007}O_4$	0.700	0.700	0.679		0.724
MM74	$Fe_{2.913\pm0.012}O_4$	0.740	0.758 ± 0.017†	0.703		
MM90	$Fe_{2.964\pm0.004}O_4$	0.892	0.899	0.895	0.880 ± 0.030†	0.880

* Uncertainty estimated to be ±0.03 as discussed in the text

† Uncertainty is one standard deviation based on three runs. Systematic error not considered.

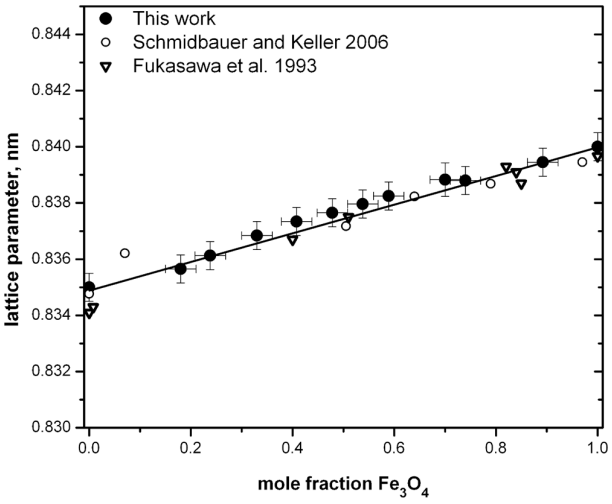

FIGURE 1. Lattice parameters of Fe_3O_4–$Fe_{8/3}O_4$ solid solutions. The values from this work are represented by filled circles, the empty circles are taken from Schmidbauer and Keller (2006), and the triangles from Fukasawa et al. (1993).

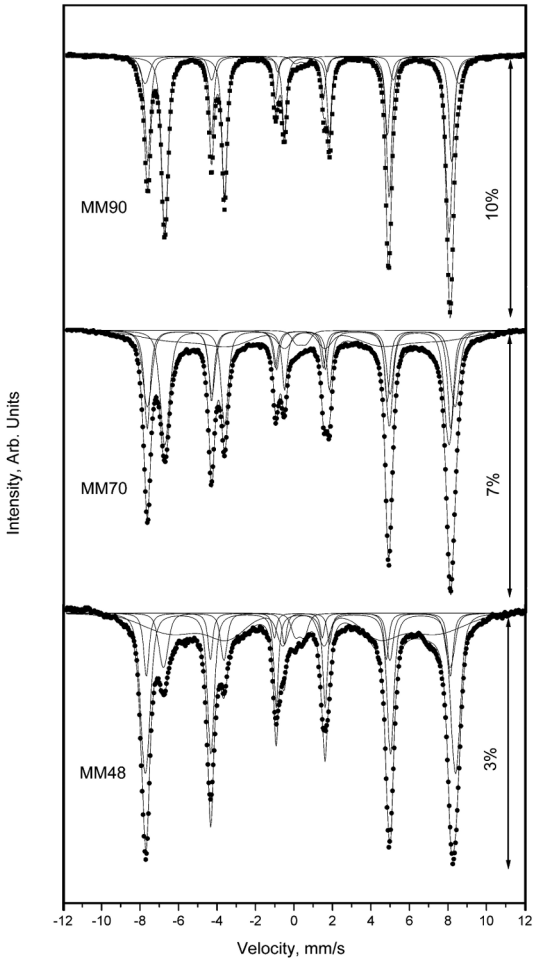

FIGURE 2. Mössbauer spectra of samples MM48, MM70, and MM90.

fitted with much less uncertainty due to absence of the broad sextet observed in MM45 and MM70 (Fig. 2). The first sextet with B_{hf1} of 50.6 T, which is the Fe signal from maghemite, has an intensity of 11%. The second sextet with B_{hf2} of 49.0 T and the third sextet with B_{hf3} of 45.8 T are from the tetrahedral site and octahedral site in magnetite, respectively, with a total intensity of 88%.

The Fe cation site occupation in samples MM24, MM54, and MM90 was investigated by analyzing the Fe $L_{2,3}$ XMCD (Figs. 3a–3c). The XMCD is the sum of the contributions from the possible cation sites where the most intense negative and positive peaks correspond to the Fe^{2+} and Fe^{3+} octahedral and Fe^{3+} tetrahedral cation sites, respectively (see Fig. 3a for peak assignment). Over the magnetite–maghemite solid solution from MM90 to MM24, analysis of the XMCD data suggests that Fe^{2+} cations are removed from Oh sites, as indicated by the reduction in the first negative peak. The Fe L_3 XMCD spectra were fitted using the weighted sum of the theoretically calculated spectra for each Fe site as shown in Figures 3d–3e. From the fitted components for the XMCD it can be seen that oxidation decreases the Fe^{2+} site occupancy (0.85 ± 0.01, 0.66 ± 0.01, and 0.43 ± 0.01 for MM90, MM54, and MM24, respectively), and increases Fe^{3+} occupancy (1.14 ± 0.01, 1.19 ± 0.01, and 1.37 ± 0.01 for MM90, MM54, and MM24, respectively) in the octahedral site. The Fe^{3+} tetrahedral site occupation is found to be close to 1.00 for MM90 and MM54, and a very slight decrease in tetrahedral site occupation is observed with sample MM24 (0.94 ± 0.01) suggesting that vacancies predominantly occupy the octahedral site, with more oxidized samples containing a very small number of vacancies in the tetrahedral site.

The mole fractions of Fe_3O_4 for MM24, MM54, and MM90 determined by XMCD are consistently slightly lower than those determined by TG/DSC. TG/DSC is a bulk technique, whereas XMCD is surface sensitive; therefore this discrepancy could be due to a slightly higher degree of oxidation at the sample surface. However, for MM90 the surface composition determined by XMCD is statistically identical to that determined for the bulk by Mössbauer (Table 1). TG/DSC values are also consistently slightly lower than bulk compositions determined by Mössbauer.

Although the reproducibility of runs on the same sample suggests an error in the magnetite mole fraction (x) about ±0.01, for each characterization, the true uncertainty is larger due to the assumptions inherent in each technique. Such error is hard to quantify but we estimate it on the order of ±0.03 in x. Within this uncertainty, the results of Mössbauer and XMCD measurements overlap those of TG. The latter are used in further calculations because they are available for all samples.

High-temperature calorimetry

Average drop solution enthalpies obtained in both solvents and temperatures for wüstite Fe_xO, $Fe_{3-y}O_4$ (MM90, MM70), stoichiometric magnetite Fe_3O_4 and hematite samples, are shown in Table 2. The drop solution enthalpy of pure iron metal pieces is obtained only in sodium molybdate, because of potential issues of lead reduction in the lead borate melt. The measured values are the sum of heat content, heat of oxidation, and heat of dissolution in the given solvent. In general, oxidation is very exothermic and is the dominant factor in the energetics. As a result, the heat ef-

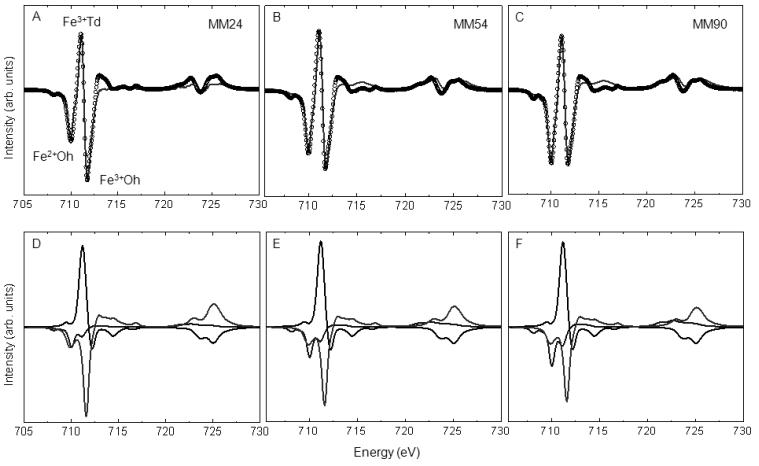

FIGURE 3. Fe $L_{2,3}$ XMCD spectra measured for MM24 (**a**), MM54 (**b**), and MM90 (**c**) (black circles) together with best-fit curves (black drawn curves). The corresponding scaled cation site components used for the best-fit curves are shown in **d**–**f**.

fects for magnetite are less positive than those for hematite and for wüstite and are exothermic in both solvents. The effect of a small amount (1.6 mol%) of a second phase (hematite) in the wüstite sample is within the experimental error. The drop solution enthalpy of $Fe_{8/3}O_4$, used in this study, was obtained previously by high-temperature oxide melt calorimetry at 973 K using sodium molybdate solvent by Laberty and Navrotsky (1998).

The only prior drop solution calorimetry measurements for magnetite in sodium molybdate solvent were performed by Laberty and Navrotsky (1998). Our value for stoichiometric magnetite (15.17 ± 0.95 kJ/mol) is in a good agreement with their data (17.1 ± 2.9 kJ/mol). It should be noted that for all drop solution enthalpies, the enthalpies of formation from the elements and the heats of mixing the uncertainty is two standard deviations from the average value.

The thermodynamic cycles used to calculate the enthalpies of oxidation at 298 K of wüstite $Fe_{0.947}O$ and magnetite $Fe_{3-y}O_4$, as well as the enthalpies of formation from elements for the three iron oxides, are shown in Table 3. The drop solution enthalpy of hematite in sodium molybdate (94.51 ± 0.93 kJ/mol), measured as described above, is in good agreement with previously measured values: 96.3 ± 0.7 (Guillemet-Fritsch et al. 2005), 93.6 ± 2.9 (Laberty and Navrotsky 1998), 95.92 ± 0.85 (Chai and Navrotsky 1994), 95.00 ± 1.8 (Drouet and Navrotsky 2003), 95.63 ± 0.50 (Majzlan et al. 2002), 95.17 ± 0.78 kJ/mol (Xu and Navrotsky 2010).

The enthalpies of formation from elements of binary oxides are calculated for the first time directly, using this newly determined independent and internally consistent set of experimental calorimetric data. Using thermodynamic cycle 3 in Table 3 and oxidative drop solution enthalpies of these oxides and of iron in molten sodium molybdate, formation enthalpies from elements were obtained (indicated with asterisk in Table 4). The enthalpy of formation from elements (–829.70 ± 2.42 kJ/mol) can also be calculated in a more indirect way (thermodynamic cycle 4, Table 3), using the drop solution enthalpies of wüstite $Fe_{0.947}O$ stoichiometric magnetite Fe_3O_4 and hematite α-Fe_2O_3 in molten lead borate, together with the enthalpy of formation of hematite, calculated from our experimental data (indicated as the pound sign in Table 4).

The enthalpies of formation from elements of non-stoichiometric $Fe_{0.947}O$, stoichiometric Fe_3O_4, and α-Fe_2O_3 obtained in this work are in very good agreement with the literature, as shown in Table 4. This methodology including oxidative drop solution of metal lumps, which have small surface area and are not prone to significant oxidation prior to calorimetry, can be extended to determine the enthalpy of formation of other binary oxides, especially in cases where such values are not accurately

TABLE 2. Wüstite, magnetite, hematite, and maghemite drop solution enthalpies (ΔH_{ds})

Sample	Phase(s)	Composition	ΔH_{ds} (kJ/mol)	ΔH_{ox} (kJ/mol)	$\Delta H_{f,el}$ (kJ/mol)
Iron	iron	Fe	–384.05 ± 2.23 (8)*	–830.51 ± 4.53	0
Wüstite	wüstite + magnetite	$Fe_{0.947}O$	–85.21 ± 0.92(8)*	–125.34 ± 1.02	–267.49 ± 1.53
			–42.68 ± 1.08(10)†	–124.17 ± 1.25	–268.49 ± 1.70
Magnetite MM70	spinel solid solution	$Fe_{2.900}O_4$	40.70 ± 1.04(8)*	–92.49 ± 1.70	–1105.50 ± 3.90
			169.11 ± 1.65(8)†	–91.47 ± 2.55	–1106.52 ± 4.34
Magnetite MM90	spinel solid solution	$Fe_{2.964}O_4$	22.38 ± 0.54(10)*	–112.78 ± 1.48	–1116.84 ± 3.88
			152.06 ± 1.61(8)†	–113.23 ± 2.56	–1116.38 ± 4.40
Magnetite	magnetite	Fe_3O_4	15.17 ± 0.95(7)*	–121.10 ± 1.69	–1123.32 ± 4.00
			147.58 ± 1.12(8)†	–120.37 ± 2.30	–1124.20 ± 4.30
Hematite	hematite	α-Fe_2O_3	94.46 ± 0.93(8)*	0	–829.70 ± 2.42
			182.29 ± 1.34(8)†		

Notes: Calculated enthalpies of oxidation (ΔH_{ox}) and enthalpies of formation from elements ($\Delta H_{f,el}$) for $Fe_{0.947}O$ and magnetite samples. The enthalpies of oxidation and formation of magnetite are calculated for sample MM90, MM70, and for stoichiometric magnetite. Error is two standard deviations of the mean. Number in parentheses is number of performed experiments.

* Indicates drop solution enthalpies obtained in molten sodium molybdate at 973 K.

† Indicates drop solution enthalpies obtained in molten lead borate at 1073 K.

known. It avoids problems sometimes encountered in combustion calorimetry, namely incomplete combustion and the formation of very fine-grained (nanophase) solid oxidation products.

The enthalpies of formation of $Fe_{0.947}O$ and Fe_3O_4, found in Robie and Hemingway (1995), Berman (1988), and Glushko et al. (1972) thermochemical tables are calculated from electrochemical data for solid buffers. Chase et al. (1985) values for both oxides are calculated from equilibrium constants of reduction reactions with CO and H_2 and from oxidation reactions with H_2O (magnetite). Our calorimetric values are the first directly measured ones.

We conclude that the enthalpies of oxidation and of formation, measured in two different solvents at two different temperatures, are consistent and in agreement with literature data. This verifies that, using the conditions of our experiments, high-temperature oxide melt calorimetry can be used to obtain thermodynamic data for Fe^{2+} compounds by oxidative drop solution calorimetry, with the final state of iron in the melt as ferric.

Lead borate at 1073 K with oxygen flushing and bubbling will provide appropriate conditions for drop solution calorimetry of iron-bearing silicates, aluminates, and aluminosilicates, borates, and phosphates. Sodium molybdate is a suitable solvent for titanates, zirconates, phosphates, tungstates, molybdates, and rare-earth containing materials. We have shown that calorimetry in sodium molybdate can be done successfully at 1073 and at 973 K with oxygen bubbling and flushing. The higher temperature may be advantageous for more refractory iron-bearing ternary oxides. Because of the ability to deal with hydrous phases under bubbling and flushing gas conditions (Navrotsky et al. 1994; Circone and Navrotsky 1992; Smelik et al. 1994; Xu et al. 2001), this methodology should also be applied to hydrated minerals containing both Fe^{2+} and Fe^{3+}, e.g., amphiboles, micas, clays, and tourmalines.

Enthalpies of mixing of Fe_3O_4–$Fe_{8/3}O_4$ solid solution

The enthalpies of mixing of the solid-solution series are calculated using the enthalpies of drop solution (Fig. 4). The drop solution enthalpy of pure maghemite is taken from Laberty and Navrotsky (1998). There is a positive deviation of the enthalpy of drop solution from the straight line connecting the two end-members, which implies a negative enthalpy of

TABLE 3. Thermodynamic cycles for $Fe_{0.947}O$ and $Fe_{3-y}O_4$

Enthalpy of oxidation		
1. $Fe_{0.947}O$ (s, 298 K) + 0.21025 O_2 (g, *T* K) → 0.4735 Fe_2O_3 (dis, *T* K)	ΔH_1	
α-Fe_2O_3 (s, 298 K) → Fe_2O_3 (dis, *T* K)	ΔH_2	
O_2 (g, 298 K) → O_2 (g, *T* K)	ΔH_3	
$Fe_{0.947}O$ (s, 298 K) + 0.21025 O_2 (g, 298 K) → 0.4735 Fe_2O_3 (solid, 298 K)	ΔH_4	
$\Delta H_4 = \Delta H_1 + 0.21025^*\Delta H_3 - 0.4735^*\Delta H_2$		
2. Fe_3O_4 (s, 298 K) + 0.25 O_2 (g, T K) → 1.5 Fe_2O_3 (dis, T K)	ΔH_6	
α-Fe_2O_3 (s, 298 K) → Fe_2O_3 (dis, *T* K)	ΔH_2	
O_2 (g, 298 K) → O_2 (g, *T* K)	ΔH_3	
Fe_3O_4 (s, 298 K) + 0.25 O_2 (g, 298 K) → 1.5 Fe_2O_3 (s, 298 K)	ΔH_7	
$\Delta H_7 = \Delta H_6 + 0.25^*\Delta H_3 - 1.5^*\Delta H_3$		
Enthalpy of formation from elements		
3. Fe_xO_y (s, 298 K) + (3x – 2y)/4 O_2 (g, *T* K) → x/2 Fe_2O_3 (dis, *T* K)	ΔH_i	i = 1, 2, 6
Fe (s, 298 K) + O_2 (g, *T* K) → Fe_2O_3 (dis, *T* K)	ΔH_8	
O_2 (g, 298 K) → O_2 (g, *T* K)	ΔH_3	
xFe (s, 298 K) + y/2 O_2 (g, 298 K) → Fe_xO_y (s, 298 K)	ΔH_9	
$\Delta H_9 = -\Delta H_i + y/2^*\Delta H_3 - x^*\Delta H_8$		
4. Fe_xO_y (s, 298 K) + (3x – 2y)/4 O_2 (g, *T* K) → x/2 Fe_2O_3 (dis, T K)	ΔH_i	i = 1, 6
α-Fe_2O_3 (s, 298 K) → Fe_2O_3 (dis, *T* K)	ΔH_2	
O_2 (g, 298 K) → O_2 (g, *T* K)	ΔH_3	
2Fe (s, 298 K) + 3/2 O_2 (g, 298 K) → Fe_2O_3 (s, 298 K)	ΔH_{10}	
xFe (s, 298 K) + (3x – 2y) O_2 (g, 298 K) → Fe_xO_y (s, 298 K)	ΔH_{11}	
$\Delta H_{11} = -\Delta H_i - y/2^*\Delta H_3 + x/2^*\Delta H_2 + x/2^*\Delta H_{10}$		

TABLE 4. Comparison of enthalpies of formation from elements at 298 K

Phase	Composition	$\Delta H_{f,el}$ (kJ/mol) This work	$\Delta H_{f,el}$ (kJ/mol)	Reference
Wüstite	$Fe_{0.947}O$	–267.49 ± 2.41*	–266.30 ± 0.80	Robie and Hemingway (1995)
		–268.49 ± 2.97†	–266.27 ± 0.84	Chase et al. (1985)
			–265.27 ± 1.67	Glushko et al. (1972)
			–265.52 ± 1.60	Darken et al. (1945)
Magnetite	Fe_3O_4	–1123.32 ± 2.42*	–1115.70 ± 3.40	Laberty and Navrotsky (1998)
		–1124.20 ± 3.00†	–1115.70 ± 2.09	Robie and Hemingway (1995)
			–1120.90 ± 0.80	Chase et al. (1985)
			–1116.90	Bichowsky and Rossini (1936)
			–1115.40	Knacke et al (1991)
			–1111.08 ± 4.18	Glushko et al. (1972)
			–1117.97 ± 1.84	Darken et al. (1945)
			–1115.70 ± 2.90	Berman (1988)
Hematite	α-Fe_2O_3	–829.70 ± 2.42*	–825.80 ± 3.20	Laberty and Navrotsky (1998)
			–826.20 ± 1.30	Robie and Hemingway (1995)
			–825.54 ± 1.30	Chase et al. (1985)
			–826.40	Knacke et al (1991)
			–822.16 ± 4.18	Glushko et al. (1972)
			–825.68 ± 1.26	Berman (1988)
			–826.00	O'Neill (1988)

* Indicates enthalpies of formation from elements, calculated using drop solution enthalpy of Fe.
† From $\Delta H_{f,el}$ (α-Fe_2O_3).

mixing. The drop solution enthalpy data can be fitted as a third-degree polynomial function, representing a subregular solution (Margules formalism). This gives:

$$\Delta H_{\text{mix}} = x(1-x)[W_1(1-x) + W_2 x] \quad (1)$$

where x is the Fe_3O_4 mole fraction and

$W_1 = -63.36 \pm 8.60$; $W_2 = -17.65 \pm 6.40$ kJ/mol.

The enthalpy of mixing curve, calculated from drop solution enthalpy data, superimposed with the experimental enthalpies of mixing is shown in Figure 5.

Discussion of magnetite-maghemite mixing properties

Three limiting cases of vacancy siting can be distinguished. The first is tetrahedral sites only, which is energetically unlikely (Lindsley 1976):

$$Fe^{3+}_{(2+x)/3}\nu_{(1-x)/3}[Fe^{2+}_x Fe^{3+}_{2-x}]O_4 \quad b=0; y=a\,. \quad (2)$$

The second is octahedral vacancies only, which is probably energetically preferable (Braun 1952; Ferguson and Hass 1958; Van Oosterhout and Rooijmans 1958; Ueda and Hasegawa 1962; Haneda and Morrish 1977) and supported by our XMCD measurements:

$$Fe^{3+}[Fe^{2+}_x Fe^{3+}_{(5-2x)/3}\nu_{(1-x)/3}]O_4 \quad a=0; y=b\,. \quad (3)$$

The third, a high-temperature limiting case, is a random distribution of vacancies on both sublattices (Armstrong et al. 1966; Annersten and Hafner 1973):

$$Fe^{3+}_{(8+x)/9}\nu_{(1-x)/9}[Fe^{2+}_x Fe^{3+}_{(16-7x)/9}\nu_{(2-2x)/9}]O_4 \quad a=1/3y\,. \quad (4)$$

For the case of octahedral vacancies, the configurational entropy is calculated, using the expression:

$$S_c = -2R\left[x\ln x + \frac{5-2x}{3}\ln\frac{5-2x}{3} + \frac{1-x}{3}\ln\frac{1-x}{3}\right]. \quad (5)$$

The entropy of mixing (difference in configurational entropy of the solid solution and that of a weighted average of configurational entropy of the end-members) is given by:

$$\Delta S_{\text{mix}} = S_c(\text{solid solutions}) - xS_c(Fe_3O_4) - (1-x)S_c(Fe_{8/3}O_4). \quad (6)$$

Analogous expressions can be developed for the cases of tetrahedral and random vacancy distribution.

The configurational entropies and entropies of mixing are shown on Figures 6a and 6b. The highest configurational entropies are obtained for randomly distributed vacancies on the two sublattices, whereas those for tetrahedral vacancies alone are lowest.

The entropies of mixing (Fig. 6b), calculated with octahedral and random vacancy distributions are approximately equal, whereas those for the tetrahedral distribution are slightly larger. In general, the location of the vacancies has a very small effect on the entropies of mixing when the Fe^{2+} and Fe^{3+} cations on octahedral sites are assumed to be distinguishable species. These small differences reflect the fact that all the cases represent highly disordered systems for which the configurational entropy varies only slowly with small changes in cation distribution and composition.

The above calculations assume that Fe^{2+} and Fe^{3+} are distinguishable species. If electron hopping is rapid, a communal entropy of electron delocalization rather than a configurational entropy, should be considered. However, there is no straightforward way of doing this at present. In addition, any magnetic effects on the entropies have not been included. Nevertheless,

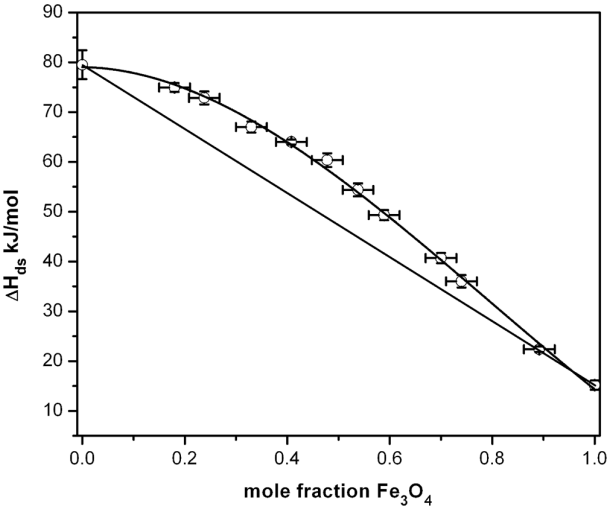

FIGURE 4. Drop solution enthalpies of Fe_3O_4–$Fe_{8/3}O_4$ solid solutions in $PbO{\cdot}B_2O_3$ at 973 K. The drop solution enthalpy of pure maghemite is taken from Laberty and Navrotsky (1998). The straight line connects the two end-members, the curve represents a *third-degree polynomial* fit of the experimental data: $y = A + B_1x + B_2x^2 + B_3x^3$. The estimated uncertainty of the magnetite mole fraction is ±0.03.

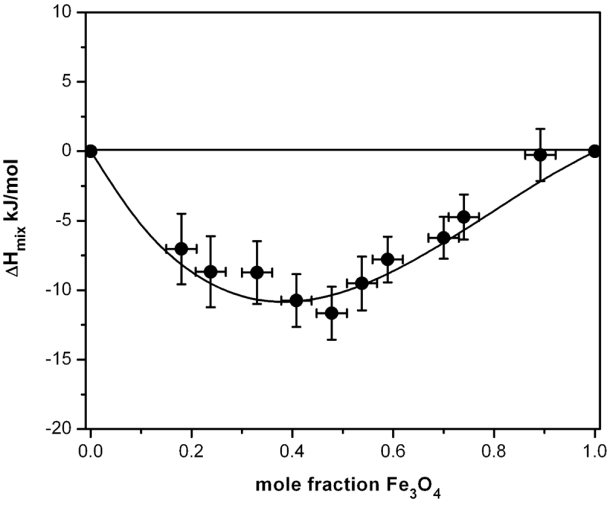

FIGURE 5. Enthalpies of mixing of Fe_3O_4–$Fe_{8/3}O_4$ solid solutions. The straight line corresponds to zero heat of mixing, the curve is calculated from $\Delta H_{\text{mix}} = x(1-x)[-63.36 \pm 8.60(1-x)+17.65 \pm 6.40x]$ kJ/mol. The estimated uncertainty of the magnetite mole fraction is ±0.03.

we believe the configurational entropy gives a reasonable first-order estimate of the entropies of mixing in the solid solution.

Gibbs free energy of mixing

The Gibbs free energy of mixing (Fig. 7) can be obtained, using the experimental enthalpies of mixing and the calculated entropies of mixing.

$$\Delta G_{mix} = \Delta H_{mix} - T\Delta S_{mix}. \quad (7)$$

The three curves obtained from the three vacancy distributions are similar, which suggest a small effect of the vacancy distribution on the free energy of mixing. The differences decrease with decreasing temperature and the three curves are almost indistinguishable at 298 K.

The thermodynamics of mixing represents contribution of both enthalpy and entropy factors. The three configurational entropy models give similar entropies of mixing, but their magnitude is significant compared to the enthalpy of mixing. For example, at 873 K, at 70 at% magnetite, ΔH_{mix} = –6.23 kJ/mol, and $T\Delta S_{mix}$ = –3.33, –2.95, and –3.05 kJ/mol for the three models, respectively.

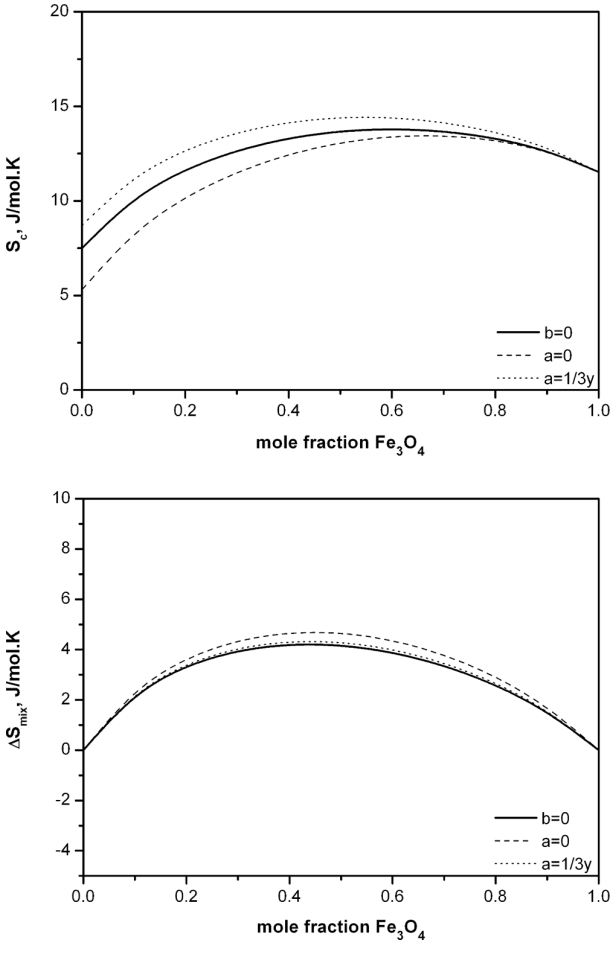

Figure 6. (**a**) Configurational entropies of Fe_3O_4–$Fe_{8/3}O_4$ solid solution. The dashed black curve represents entropies, calculated for tetrahedral vacancy distribution; the thick curve = for octahedral and the dotted curve = for random. (**b**) Entropies of mixing of Fe_3O_4–$Fe_{8/3}O_4$ solid solution. The dashed black curve represents entropies, calculated for tetrahedral vacancy distribution; the thick curve is for octahedral and the dotted curve for random.

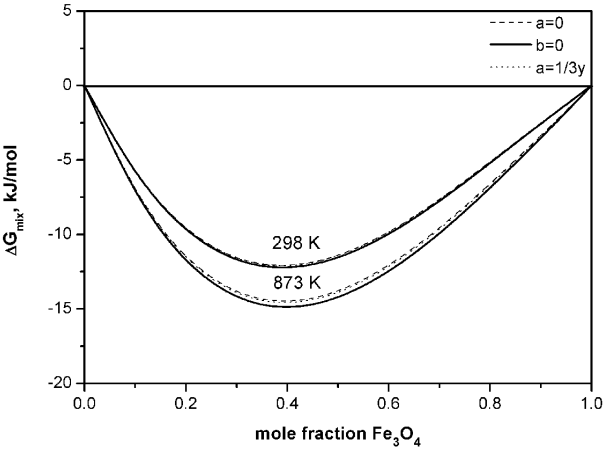

Figure 7. Gibbs free energy of mixing of Fe_3O_4–$Fe_{8/3}O_4$ solid solution at 298 and 873 K. The straight line corresponds to zero. The dashed black curve is calculated, using configurational entropies calculated for tetrahedral vacancy distribution; the thick curve is for octahedral and the dotted curve for random.

These results point to general important conclusions. First, since the enthalpy of mixing is exothermic (stabilizing) and the entropy of mixing is also favorable and is a smooth curve, there is no reason to expect phase separation at any temperature. Second, given the high degree of disorder in the system, differences in calculated free energies of mixing for the three cation distribution models are minor. Consistent with the XMCD data and previous studies, the octahedral vacancy model is preferable.

We conclude that the calorimetric methodology discussed here provides accurate data for phases containing ferric and ferrous iron, as applied in the magnetite–maghemite solid solutions, and we anticipate applications to complex mineral phases in the future.

Acknowledgments

Financial support from DOE grants DE-FG02-97ER14749 and DEAC02-98CH10886 are gratefully acknowledged. K.M.R. and C.I.P. gratefully acknowledge support from the Pacific Northwest National Laboratory Science Focus Area (SFA) Subsurface Biogeochemical Research (SBR) Program of the U.S. Department of Energy (DOE). The authors thank Elke Arenholz and Juan Liu for assistance with the XA and XMCD measurements, performed at the Advance Light Source supported by the DOE Office of Science, Office of Basic Energy Sciences under contract no. DE-AC02-05CH11231.

References cited

Akaogi, M., Ito, E., and Navrotsky, A. (1989) Olivine-modified spinel-spinel transformaions in the system Mg_2SiO_4–Fe_2SiO_4: Calorimetric measurements, thermochemical calculations, and geophysical application. Journal of Geophysical Research, 94, 15671–15685.

Annersten, H. and Hafner, S.S. (1973) Vacancy distribution in synthetic spinels of the series Fe_3O_4-γ-Fe_2O_3. Zeitschrift für Kristallographie, Kristallgeometrie, Kristallphysik, Kristallchemie, 137, 321–340.

Arenholz, E. and Prestemon, S.O. (2005) Design and performance of an eight-pole resistive magnet for soft X-ray magnetic dichroism measurements. Review of Scientific Instruments, 76, 083908.

Armstrong, R.J., Morrish, A.H., and Sawatzky, G.A. (1966) Mössbauer study of ferric ions in the tetrahedral and octahedral sites of a spinel. Physics Letters, 23, 414–416.

Asao, H., Ono, K., Yamaguchi, A., and Moriyama, J. (1970) Thermodynamic properties of wüstite (FeO_{1+y}). Memoirs of the Faculty of Engineering, Kyoto University, 32, 66–77.

Bauminger, R., Cohen, S.G., Marinov, A., Ofer, S., and Segal, E. (1961) Study of the low temperature transition in magnetite and the internal fields acting on iron nuclei in some spinel ferrites, using Mössbauer absorption. Physical Review, 122, 1447–1450.

Belin, T., Guigue-Millot, N., Caillot, T., Aymes, D., and Niepce, J.C. (2002) Influence of grain Size, oxygen stoichiometry, and synthesis conditions on the γ-Fe_2O_3 vacancies ordering and lattice parameters. Journal of Solid State Chemistry, 163, 459–465.

Berman, R.G. (1988) Internally-consistent thermodynamic data for minerals in the system Na_2O–K_2O–CaO–MgO–FeO–Fe_2O_3–Al_2O_3–SiO_2–TiO_2–H_2O–CO_2. Journal of Petrology, 29, 445–522.

Bettahar, N., Conflant, P., Abraham, F., and Thomas, D. (1987) Pb_2PtO_4, a new platinum-lead oxide with edge-shared PtO_6 octahedral chains. Journal of Solid State Chemistry, 67, 85–90.

Bichowsky, F. and Rossini, D., Eds. (1936) The Thermochemistry of Chemical Substances, 460 p. Reinold, New York.

Bomati-Miguel, O., Mazeina, L., and Navrotsky, A. (2008) Calorimetric study of maghemite nanoparticles synthesized by laser-induced pyrolysis. Chemistry of Materials, 20, 591–598.

Boudeulle, M., Batis-Landoulsi, H., Leclercq, C., and Vergnon, P. (1983) Structure of γ-ferric oxide microcrystals: vacancy distribution and superstructure. Journal of Solid State Chemistry, 48, 21–32.

Braun, P.B. (1952) Superstructure in spinels. Nature, 170, 1123.

Brown, N. and Navrotsky, A. (1994) Hematite–ilmenite (Fe_2O_3–$FeTiO_3$) solid solutions: The effects of cation ordering on the thermodynamics of mixing. American Mineralogist, 79, 485–496.

Carel, C. and Vallet, P. (1981) First-order transition of magnetite at 1160 °C. Bulletin de la Societe Scientifique de Bretagne, 52, 55–59.

Chai, L. and Navrotsky, A. (1994) Enthalpy of formation of siderite and its application in phase equilibrium calculation. American Mineralogist, 79, 921–929.

——— (1996a) Synthesis, characterization, and energetics of solid solution along the dolomite–ankerite join, and implications for the stability of ordered $CaFe(CO_3)_2$. American Mineralogist, 81, 1141–1147.

——— (1996b) Synthesis, characterization, and enthalpy of mixing of the (Fe,Mg) CO_3 solid solution. Geochimica et Cosmochimica Acta, 60, 4377–4383.

Chase, M.W. Jr., Davies, C.A., Downey, J.R. Jr., Frurip, D.J., McDonald, R.A., and Syverud, A.N. (1985) JANAF Thermochemical Tables. Third edition. Part II. Cr–Zr. Journal of Physical and Chemical Reference Data 14 (Suppl. 1).

Chatillon-Colinet, C., Newton, R.C., Perkins, D., and Kleppa, O.J. (l983) Enthalpy of formation of $Fe_3Al_2Si_3O_{12}$ (almandine) by high temperature alkali borate solution calorimetry. Geochimica et Cosmochimica Acta, 47, 1597–1603.

Chen, C.T., Idzerda, Y.U., Lin, H.J., Smith, N.V., Meigs, G., Chaban, E., Ho, G.H., Pellegrin, E., and Sette, F. (1995) Experimental confirmation of the X-ray magnetic circular dichroism. Sum rules for iron and cobalt. Physical Review Letters, 75, 152–155.

Circone, S. and Navrotsky, A. (1992) Substitution of $^{[6,4]}$Al in phlogopite: High-temperature solution calorimetry, heat capacities and thermodynamic properties of the phlogopite-eastonite join. American Mineralogist, 77, 1191–1205.

Coey, J.M.D. and Morrish, A.H. (1971) Mössbauer study of conduction in magnetite. Journal de Physique, Colloque 1, Cl-271–Cl-273.

Cook, D.C., Oh, S.J., Balasubramanian, R., and Yamashita, M. (1999) The role of goethite in the formation of the protective corrosion layer on steels. Hyperfine Interactions, 122, 59–70.

Cormack, A.N. (1983) A perfect lattice approach to non-stoichiometry. Solid State Ionics, 8, 187–192.

Cornell, R.M. and Schwertmann, U., Eds. (2003) The Iron Oxides: Structure, properties, reactions, occurrences and uses, 664 p. Wiley-VCH, Darmstadt.

Da Costa, G.M., De Grave, E., Bryan, A.M., and Bowen, L.H. (1994) Mössbauer studies of nano-sized aluminum-substituted maghemites. Hyperfine Interactions, 94, 1983–1987.

Da Costa, G.M., De Grave, E., and Vandenberghe, R.E. (1998) Mössbauer studies of magnetite and Al-substituted maghemites. Hyperfine Interactions, 117, 207–243.

Darken, L.S. and Gurry, R.W. (1945) The system iron–oxygen. I. The wüstite field and related equilibria. Journal of the American Chemical Society, 67, 1398–1412.

——— (1946) The system iron–oxygen. II. Equilibrium and thermodynamics of liquid oxide and other phases. Journal of the American Chemical Society, 68, 798–819.

Drouet, C. and Navrotsky, A. (2003) Synthesis, characterization, and thermochemistry of K–Na–H_3O jarosites. Geochimica et Cosmochimica Acta, 67, 2063–2076.

Dunn, D.S., Bogart, M.B., Brossia, C.S., and Cragnolino, G.A. (2000) Corrosion of iron under alternating wet and dry conditions. Corrosion, 56, 470–480.

Esdaile, J.D. (1983) The correlation of the thermodynamic properties of wüstite by a Gaussian based formalism. Metallurgical Transactions A: Physical Metallurgy and Materials Science, 14, 771–775.

Fabrichnaya, O.B. and Sundman, B. (1997) The assessment of thermodynamic parameters in the Fe–O and Fe–Si–O systems. Geochimica et Cosmochimica Acta, 61, 4539–4555.

Ferguson, G.A. and Hass, M. (1958) Magnetic structure and vacancy distribution in γ-Fe_2O_3 by neutron diffraction. Physical Review, 112, 1130–1131.

Fukasawa, T., Iwatsuki, M., and Furukawa, M. (1993) State analysis and relationship between lattice constants and compositions including minor elements of synthetic magnetite and maghemite. Analytica Chimica Acta, 281, 413–419.

Gallagher, K.J., Feitknecht, W., and Mannweller, U. (1968) Mechanism of oxidation of magnetite to γ-Fe_2O_3. Nature, 217, 1118–1121.

——— (1970) Mechanism for the oxidation of Fe_3O_4. Nature, 228, 548–549.

Gillot, B., Rousset, A., and Dupre, G. (1978) Influence of crystallite size on the oxidation kinetics of magnetite. Journal of Solid State Chemistry, 25, 263–271.

Glushko, V.P., Medvedev, V.A., Bergman, G.A., Vasilev, B.P., Gurvich, L.V., Alekseev, V.I., Kolesov, V.P., Yungman, V.S., Ioffe, N.T., Vorabev, A.F., and others. (1972) Thermicheskie konstanty veshchestv. Academy of Science, Russia.

Goursat, A.G. and Smeltzer, W.W. (1973) Oxidation of iron. Reviews on High-Temperature Materials, 1, 351–396.

Goss, C.J. (1988) Saturation magnetisation, coercivity and lattice parameter changes in the system Fe_3O_4–γ-Fe_2O_3, and their relationship to structure. Physics and Chemistry of Minerals, 16, 164–171.

Gota, S., Gautier-Soyer, M., and Sacchi, M. (2000) Fe 2*p* absorption in magnetic oxides: Quantifying angular-dependent saturation effects. Physical Review B, 62, 4187–4190.

Greaves, C. (1983) A powder neutron diffraction investigation of vacancy ordering and covalence in γ-ferric oxide. Journal of Solid State Chemistry, 49, 325–333.

Groenvold, F. and Sveen, A. (1974) Heat capacity and thermodynamic properties of synthetic magnetite (Fe_3O_4) from 300 to 1050 K. Ferrimagnetic transition and zero point entropy. Journal of Chemical Thermodynamics, 6, 859–872.

Guillemet-Fritsch, S., Navrotsky, A., Tailhades, P., Coradin, H., and Wang, M. (2005) Thermochemistry of iron manganese oxide spinels. Journal of Solid State Chemistry, 178, 106–113.

Haavik, C., Stølen, S., Fjellvåg, H., Hanfland, M., and Häusermann, D. (2000) Equation of state of magnetite and its high-pressure modification: thermodynamics of the Fe–O system at high pressure. American Mineralogist, 85, 514–523.

Hägg, G. (1935) The crystal structure of magnetic ferric oxide, γ-Fe_2O_3. Zeitschrift fur Physikalische Chemie, Abteilung B: Chemie der Elementarprozesse, Aufbau der Materie, 29, 95–103.

Haneda, K. and Morrish, A.H. (1977) Vacancy ordering in γ-Fe_2O_3 small particles. Solid State Communication, 22, 779–782.

Haul, R. and Schoon, T. (1939) Structure of ferromagnetic ferric oxides, γ-Fe_2O_3. Zeitschrift fur Physikalische Chemie, 844, 216–226.

Hemingway, B.S. (1990) Thermodynamic properties for bunsenite, NiO, magnetite, Fe_3O_4, and hematite, Fe_2O_3, with comments on selected oxygen buffer reactions. American Mineralogist, 75, 781–790.

Holland, T.J.B. and Powell, R. (1998) An internally consistent thermodynamic data set for phases of petrological interest. Journal of Metamorphic Geology, 16, 309–343.

Jacob, K.T., Rajitha, G., and Kale, G.M. (2009) Thermodynamic properties of Pb_2PtO_4 and $PbPt_2O_4$ and phase equilibria in the system Pb–Pt–O. Journal of Alloys and Compounds, 481, 228–232.

Janowski, J., Benesch, R., Jaworski, M., and Miklasinski, A. (1970a) Thermodynamic properties of wüstite obtained by oxidizing pure iron. Metalurgia i Odlewnictwo, 37, 11–28.

Janowski, J., Benesch, R., Bialek, H., Dargel, L., Jaworski, M., Kolodziejczyk, A., Miklasinski, A., and Obuszko, Z. (1970b) Determination of thermodynamic properties and structure of wüstite by measuring some physical quantities. Metalurgia i Odlewnictwo, 38, 7–32.

Knacke, O., Kubaschewski, O., and Hesselmann, K., Eds. (1991) Thermochemical Properties of Inorganic Substances. second edition, 688 p. Springer-Verlag, Berlin.

Kojitani, H. and Akaogi, M. (1994) Calorimetric study of olivine solid solutions in the system Mg_2SiO_4–Fe_2SiO_4. Physics and Chemistry of Minerals, 20, 536–540.

Komarov, V.F., Oleinikov, N.N., and Tretyakov, Yu.D. (1967) Thermodynamic properties of solid solutions based on hematite in an iron–oxygen system. Izvestiya Akademii Nauk SSSR, Neorganicheskie Materialy, 3, 1064–1072.

Kryukova, G.N., Chuvilin, A.L., and Sadykov, V.A. (1990) On the γ-ferric oxide superstructure observation by high resolution electron microscopy. Journal of Solid State Chemistry, 89, 208–211.

Kullerud, G., Donnay, G., and Donnay, J.D.H. (1969) Omission solid solution in magnetite: kenotetrahedral magnetite. Zeitschrift für Kristallographie, Kristallgeometrie, Kristallphysik, Kristallchemie, 128, 1–17.

Kündig, W. and Hargrove, R.S. (1969) Electron hopping in magnetite. Solid State Communications, 7, 223–227.

Kurepin, V.A (1975) Activity of components, thermodynamical characteristics of reactions, and phase equilibriums in the iron–oxygen system at high temperatures and pressures. Geokhimiya, 10, 1475–1483 (in Russian).

Laberty, C. and Navrotsky, A. (1998) Energetics of stable and metastable low-temperature iron oxides and oxyhydroxides. Geochimica et Cosmochimica Acta, 62, 2905–2913.

Leonovich, B.I., Lykasov, A.A., and Platonova, O.V. (2001) Thermodynamic analysis of iron–oxygen system. Izvestiya Vysshikh Uchebnykh Zavedenii, Chernaya Metallurgiya, 6, 3–7.

Lindsley, D.H. (1976) The crystal chemistry and structure of oxide minerals as exemplified by the Fe–Ti oxides. In D. Rumble, Ed., Oxide Minerals, 3, p. L-1–L-60. Reviews in Mineralogy, Mineralogical Society of America, Chantilly, Virginia.

Lindsley, D.H., Ed. (1991) Oxide Minerals: Petrologic and Magnetic Significance, vol. 25, 509 p. Reviews in Mineralogy, Mineralogical Society of America, Chantilly, Virginia.

Linton, J., Navrotsky, A., and Fei, Y. (1998) The thermodynamics of ordered perovskites on the $CaTiO_3$–$FeTiO_3$ join. Physics and Chemistry of Minerals, 25, 591–596.

Majzlan, J., Navrotsky, A., and Neil, J.M. (2002) Energetics of anhydrite, barite, celestine, and anglesite: A high-temperature and differential scanning calorimetry study. Geochimica et Cosmochimica Acta, 66, 1839–1850.

Majzlan, J., Grevel, K.D., and Navrotsky, A. (2003) Thermodynamics of Fe oxides: Part II. Enthalpies of formation and relative stability of goethite (α-FeOOH), lepidocrocite (γ-FeOOH), and maghemite (γ-Fe_2O_3). American Mineralogist, 88, 855–859.

Marucco, J.F., Gerdanian, P., and Dodé, M. (1970) Determination of partial molar values of an oxygen mixture in ferrous oxide at 1075 °C. I. Direct measurements of partial molar enthalpies of an oxygen mixture using a Tian-Calvet-type high-temperature microcalorimeter. Journal de Chimie Physique et de Physico-Chimie Biologique, 67, 906–912.

Mehta, A., Leinenweber, K., Navrotsky, A., and Akaogi, M. (1994) Calorimetric study of high pressure polymorphism in $FeTiO_3$: Stability of the perovskite phase. Physics and Chemistry of Minerals, 21, 207–212.

Morales, M.P., Pecharroman, C., Gonzalez Carreno, T., and Serna, C.J. (1994) Structural characteristics of uniform γ-Fe_2O_3 particles with different axial (length/width) ratios. Journal of Solid State Chemistry, 108, 158–163.

Morris, R.V., Golden, D.C., Bell, J.F. III, Shelfer, T.D., Scheinost, A.C., Hinman, N.W., Furniss, G., Mertzman, S.A., Bishop, J.L., Ming, D.W., Allen, C.C., and Britt, D.T. (2000) Mineralogy, composition, and alteration of Mars Pathfinder rocks and soils: Evidence from multispectral, elemental, and magnetic data on terrestrial analogue, SNC meteorite, and Pathfinder samples. Journal of Geophysical Research [Planets], 105 (E1), 1757–1817.

Navrotsky, A. (1977) Progress and new directions in high temperature calorimetry. Physics and Chemistry of Minerals, 2, 89–104.

——— (1997) Progress and new directions in high-temperature calorimetry revisited. Physics and Chemistry of Minerals, 24, 222–241.

Navrotsky, A., Pintchovski, F.S., and Akimoto, S.I. (1979) Calorimetric study of the stability of high pressure phases in the systems CoO–SiO_2 and "FeO"–SiO_2, and calculation of phase diagrams in MO SiO_2 systems. Physics of the Earth and Planetary Interiors, 19, 275–292.

Navrotsky, A., Rapp, R.P., Smelik, E., Burnley, P., Circone, S., Chai, L., Bose, K., and Westrich, H.R. (1994) The behavior of H_2O and CO_2 in high-temperature lead borate solution calorimetry of volatile-bearing phases. American Mineralogist, 79, 1099–1109.

Navrotsky, A., Dooley, D., Reeder, R., and Brady, P. (1999) Calorimetric studies of the energetics of order-disorder in the system $Mg_{1-x}Fe_xCa(CO_3)_2$. American Mineralogist, 84, 1622–1626.

Néel, L. (1948) Propriétés magnétiques des ferrites. Ferrimagnétisme et antiferromagnétisme. Annales de Physique, 3, 137–198.

Neff, D., Dillmann, P., Bellot-Gurlet, L., and Beranger, G. (2004) Corrosion of iron archaeological artefacts in soil: characterisation of the corrosion system. Corrosion Science, 47, 515–535.

Noguchi, T. and Nakamura, T. (2000) Mineralogy of antarctic micrometeorite recovered from the Dome Fuji Station. Antarctic Meteorite Research, 13, 285–301.

O'Neill, H.St.C. (1988) Systems Fe–O and Cu–O: Thermodynamic data for the equilibria Fe–"FeO", Fe–Fe_3O_4, "FeO"–Fe_3O_4, $Fe3O_4$–Fe_2O_3, Cu–Cu_2O, and Cu_2O–CuO from emf measurements. American Mineralogist, 73, 470–486.

Pattrick, R.A.D., van der Laan, G., Henderson, C.M.B., Kuiper, P., Dudzik, E., and Vaughan, D.J. (2002) Cation site occupancy in spinel ferrites studied by X-ray magnetic circular dichroism: developing a method for mineralogists. European Journal of Mineralogy, 14, 1095–1102.

Pearce, C.I., Henderson, C.M.B., Telling, N.D., Pattrick, R.A.D., Charnock, J.M., Coker, V.S., Arenholz, E., Tuna, F., and van der Laan, G. (2010) Fe site occupancy in magnetite–ulvospinel solid solutions: A new approach using X-ray magnetic circular dichroism. American Mineralogist, 95, 425–439.

Peterson, M.L., White, A.F., Brown, G.E. Jr., and Parks, G.A. (1997) Surface passivation of magnetite by reaction with aqueous Cr(IV): XAFS and TEM results. Environmental Science and Technology, 31, 1573–1576.

Raccah, P. and Vallet, P. (1962) Thermodynamic properties of wüstite, a solid solution of iron and oxygen. Comptes Rendus de l'Académie des Sciences, 254, 1038–1040.

Ringwood, A.E. (1977) Composition of he core and implications for origin of the earth. Geochemistry Journal, 11, 111–135.

Rizzo, H.F., Gordon, R.S., and Cutler, I.B. (1968) Determination of thermodynamic properties in single-phase wüstite by coulometric titration in a high-temperature galvanic cell. National Bureau of Standards, 296, 129–142.

——— (1969) Determination of phase boundaries and thermodynamic functions in the iron–oxygen system by E.M.F. measurements. Journal of the Electrochemical Society, 116, 266–274.

Robie, R.A. and Hemingway, B.S. (1995) Thermodynamic properties of minerals and related substances at 298.15 K and 1 bar (105 Pascals) pressure and at higher temperatures, 461 p. U.S. Geological Survey Bulletin, no. 2131.

Schmidbauer, E. and Keller, M. (2006) Magnetic hysteresis properties, Mössbauer spectra and structural data of spherical 250 nm particles of solid solutions Fe_3O_4 γ-Fe_2O_3. Journal of Magnetism and Magnetic Materials, 297, 107–117.

Scott, T.B., Allen, G.C., Heard, P.J., and Randell, M.G. (2005) Reduction of U(VI) to U(IV) on the surface of magnetite. Geochimica et Cosmochimica Acta, 69, 5639–5646.

Shebanova, O.N. and Lazor, P. (2003) Raman study of magnetite (Fe_3O_4): laser-induced thermal effects and oxidation. Journal of Raman Spectroscopy, 34, 845–852.

Shmakov, A.N., Kryukova, G.N., Tsybulya, S.V., Chuvilin, A.L., and Solovyeva, L.P. (1995) Vacancy ordering in γ-Fe_2O_3: Synchrotron X-ray powder diffraction and high-resolution electron microscopy studies. Journal of Applied Crystollography, 28, 141–145.

Sinha, K.P. and Sinha, A.P.B. (1957) Ein Fehlstellenüberstruktur-Modell für γ-Fe_2O_3. Zeitschrift für Anorganische und Allgemeine Chemie, 293, 228–232.

Smelik, E., Jenkins, D.M., and Navrotsky, A. (1994) A calorimetric study of synthetic amphiboles along the tremolite-tschermakite join and the heats of formation of magnesiohornblende and tschermakite. American Mineralogist, 79, 1110–1122.

Snow, C.L., Lee, C.R., Shi, Q., Boerio-Goates, J., and Woodfield, B.F. (2010) Size-dependence of the heat capacity and thermodynamic properties of hematite (α-Fe_2O_3). Journal of Chemical Thermodynamics, 42, 1142–1151.

Spencer, P.J. and Kubaschewski, O. (1978) A thermodynamic assessment of the iron–oxygen system. CALPHAD: Computer Coupling of Phase Diagrams and Thermochemistry, 2, 147–167.

Stohr, J. (1995) X-ray magnetic circular dichroism spectroscopy of transition metal thin films. Journal of Electron Spectroscopy and Related Phenomena, 75, 253–272.

Stølen, S., Glöckner, R., Grønvold, F., Atake, T., and Izumisawa, S. (1996) Heat capacity and thermodynamic properties of nearly stoichiometric wüstite from 13 to 450 K. American Mineralogist, 81, 973–981.

Sundman, B. (1991) An assessment of the iron–oxygen system. Journal of Phase Equilibria, 12, 127–140.

Takai, S., Akishige, Y., Kawaji, H., Atake, T., and Sawaguchi, E. (1994) Low-temperature heat capacities and Verwey transition of magnetite. Journal of Chemical Thermodynamics, 26, 1259–1266.

Takei, H. and Chiba, S. (1966) Vacancy ordering in epitaxially-grown single crystals of γ-Fe_2O_3. Journal of the Physical Society of Japan, 21, 1256–1263.

Tessier F., Navrotsky, A., Niewa, R., Leineweber, A., Jacobs, H., Kikkawa, S., Takahashi, M., Kanamaru, F., DiSalvo, F.J. (2000) Energetics of binary iron nitrides. Solid State Sciences, 2, 457–462.

Thierry, P., Chatillon-Colinet, C., Mathieu, J.C., Regnard, J.R., and Amosse, J. (1981) Thermodynamic properties of the forsterite–fayalite (Mg_2SiO_4–Fe_2SiO_4) solid solution. Determination of heat of formation. Physics and Chemistry of Minerals, 7, 43–46.

Ueda, R. and Hasegawa, K. (1962) Vacancy distribution in γ-Fe_2O_3. Journal of the Physical Society of Japan, 17, Suppl. BII, 391–394.

Vallet, P. (1975a) Thermodynamic properties of solid wüstite below 911 °C. Comptes Rendus des seances de l'Academie des Sciences, Serie C: Sciences Chimiques, 280, 239–241.

——— (1975b) Thermodynamic properties of solid wüstite at temperatures over 911 °C. Comptes Rendus des seances de l'Academie des Sciences, Serie C: Sciences Chimiques, 281, 291–294.

Vallet, P. and Carel, C. (1986) Evaluation of molar thermodynamic properties of wüstite solids from their equilibrium thermogravimetric study. Part 1. Formulation of partial molar and integral magnitudes of three W_I and three W_I^{II}. Revue de Chimie Minerale, 23, 362–377.

Vallet, P., Kleman, M., and Raccah, P. (1963) New thermodynamic properties and a new diagram for solid wüstite. Comptes rendus hebdomadaires des séances de l'Académie des Sciences, 256, 136–138.

Vandenberghe, R.E. and De Grave, E. (1989) Mössbauer studies of oxidic spinels. Mössbauer Spectroscopy Applied to Inorganic Chemistry, 3, 159–182.

Van der Laan, G. and Kirkman, I.W. (1992) The 2p absorption-spectra of 3d transition-metal compounds in tetrahedral and octahedral symmetry. Journal of Physics-Condensed Matter, 4, 4189–4204.

Van der Laan, G. and Thole, B.T. (1991) Strong magnetic-X-ray dichroism in 2p absorption-spectra of 3d transition-metal ions. Physical Revew B, 43, 13401–13411.

Van der Laan, G., Zaanen, J., Sawatzky, G.A., Karnatak, R.C., and Esteva, J.M. (1986) Comparison of X-ray absorption with X-ray photoemission of nickel dihalides and NiO. Physical Revew B, 33, 4253–4263.

van Oorschot, I.H.M. and Dekkers, M.J. (1999) Dissolution behaviour of fine-grained magnetite and maghemite in the citrate–bicarbonate–dithionite extraction method. Earth and Planetary Science Letters, 167, 283–295.

Van Oosterhout, G.W. and Rooijmans, C.J.M. (1958) A new superstructure in γ-ferric oxide. Nature, 181, 44–45.

Verwey, E.J.W. (1939) Electronic conduction of magnetite (Fe_3O_4) and its transition point at low temperatures. Nature, 144, 327–328.

Verwey, E.J.W. and de Boer, J.H. (1936) Cation arrangement in a few oxides with crystal structures of the spinel type. Recueil des Travaux Chimiques des Pays-Bas et de la Belgique, 55, 531–540.

Weber, H.P. and Hafner, S.S. (1971) Vacancy distribution in nonstoichiometric magnetites. Zeitschrift für Kristallographie, 133, 327–340.

Westrum, E.F. and Groenvold, F. (1969) Fe_3O_4 heat capacity and thermodynamic properties from 5 to 350 K, low-temperature transition. Journal of Chemical Thermodynamics, 1, 543–557.

White, A.F. and Peterson, M.L. (1996) Reduction of aqueous transition metal species on the surfaces of Fe(II)-containing oxides. Geochimimica et Cosmochimica Acta, 60, 3799–3814.

Wood, B.J. and Kleppa, O.J. (1981) Thermochemistry of forsterite–fayalite olivine solutions. Geochimica et Cosmochimica Acta, 45, 529–534.

Xu, F. and Navrotsky, A. (2010) Enthalpies of formation of pyrrhotite $Fe_{1-0.125x}S$ ($0 \le x \le 1$) solid solutions. American Mineralogist, 95, 717–723.

Xu, H., Zhang Y., and Navrotsky, A. (2001) Enthalpies of formation of microporous titanosilicates ETS-4 and ETS-10. Microporous and Mesoporous Materials, 47, 285–291.

Manuscript received May 12, 2011
Manuscript accepted Don Baker
Manuscript handled by September 14, 2011